DRAFT VERSION DECEMBER 19, 2022
Typeset using LaTeX **twocolumn** style in AASTeX631

Dust continuum observations towards NGC 2024 FIR 5/6

STAR FORMATION GROUP,[1,2,3] HAN-TSUNG LEE,[1,2] HSIEN-JU TSAI,[3] AND TAI-SHAN CHEN[3]

[1]*Department of Physics, National Taiwan University, No. 1, Sec. 4, Roosevelt Rd., Taipei 10617, Taiwan, R.O.C.*
[2]*Institute of Astronomy and Astrophysics, Academia Sinica, 11F of Astronomy-Mathematics Building, AS/NTU No.1, Sec. 4, Roosevelt Rd, Taipei 10617, Taiwan, ROC*
[3]*Department of Earth Sciences, National Taiwan Normal University, 162, Section 1, Heping E. Rd., Taipei City 106, Taiwan*

ABSTRACT

We have performed the dust continuum observations towards the low mass star-forming regions NGC 2024 FIR 5 and FIR 6 at 1.3 mm using the Submillimeter Array. We compare the geometries seen at 1.3 mm with those from different wavelengths with similar resolutions of 1–2" and measure the spectral index. Although with a $\theta_{\rm maj} \times \theta_{\rm min}$=1.30"×1.03" synthesized beam, our observation cannot resolve the binary core FIR 5. The FIR 6 is spatially resolved to two compact sources FIR 6C and FIR 6N. The observed flux density $F_{225\,\rm GHz}$ is 513, 340 and 41 mJy for FIR 5, FIR 6C and FIR 6N, respectively. The spectral energy distribution (SED) fitting gives a spectral index $\alpha \sim 2.6$ for FIR 5, and $\alpha \sim 1.7$ for FIR 6N, which suggests that millimeter continuum of FIR 5 is dominated by thermal dust emission, while that of FIR 6C could possibly be dominated by free-free emission.

Keywords: ISM: individual objects (NGC 2024) – stars: formation – techniques: interferometric

1. INTRODUCTION

The target source we chose is the NGC 2024 Flame Nebula located in the Orion constellation, about 400–500 pc away from the earth. In Barnard's Loop of Orion, besides the famous M42 Orion Nebula and Barnard 33 Horsehead Nebula, there is also this NGC 2024 Emission Nebula. Due to the high-energy ultraviolet radiation from the nearby blue giant star Alnitak, the hydrogen in these large-scale molecular clouds is ionized, and the electrons combine with hydrogen ions to produce light. The darker gas and dust block the light, causing this nebula to take on a flame-like attitude.

In this work, we investigate low mass star-forming regions FIR 5 and FIR 6 in NGC 2024. FIR 5 harbors a binary system SMM1 and SMM2 in class 0 phases with masses of 1.7 $M_\odot$ and 0.7 $M_\odot$ and a separation of ∼4" from previous SMA observations at 850 μm (Alves et al. 2011). FIR 6 which comprises two dense cores FIR 6C and FIR 6N is accidentally imaged in our field-of-view as well. FIR 6 is detected in class I methanol maser lines (Choi et al. 2012a). The physical nature of the brighter source FIR 6C is still unknown, while it is argued to contain a hypercompact HII region ionized by an B1 star (Choi et al. 2012b). The fainter source FIR 6N is likely a class 0 source driving a very young outflow with ∼400 yr age (Richer 1990). Our goal is to compare morphology of FIR 5 and FIR 6 at 1.3 mm and at other wavelengths presented in the literature and study origins of their millimeter continuum from spectral energy distribution (SED) analysis.

Details of our SMA observations are introduced in Section 2. The results are presented in Section 3.

2. OBSERVATIONS

We have performed the SMA observations of NGC 2024 FIR 5 at 1.3 mm band on November 9^{th}, 2022. The array configuration of this observation is 'extended' that covers the baseline length from 24.635 to 165.514 $k\lambda$, and the phase center is RA, Dec = $05^h41^m44^s.3$, -01°55′38.″0 (J2000). Dual polarization mode of the SMA Wideband Astronomical ROACH2 Machine (SWARM) backend is used. ely. The intrinsic spectral channel width is 140 kHz. The RxA receivers cover frequency ranges of 207.386–219.687 GHz and 227.388–239.688 GHz in lower and upper sidebands; The RxB receivers cover frequency ranges of 223.387–235.688 GHz and 243.389–255.689 GHz in lower and upper sidebands. With the spectral setup, the S2 chunk in the upper sideband of the RxA receiver and S3 chunk in the lower sideband of the RxB receiver are centered at CO (2-1) line with a rest frequency of 230.538 GHz.

The data reduction was done following the standard data calibration strategy of SMA. The application of Tsys information and the absolute flux, passband, and gain calibrations were carried out using the MIR IDL software package (Qi 2003). The absolute flux scaling was derived by comparing the visibility amplitudes of the gain calibrator 0501-019 with those of the absolute flux calibrator, Neptune. The bandpass calibrator is 1924-292. We nominally quote the ∼15% typical absolute flux calibration error of SMA. All the observation details are shown in Table 1.

Continuum imaging was done using CLEAN algorithm in the Miriad software package (Sault et al. 1995). To reach a better signal-to-noise ratio, we combined all available calibrated data. Surprisingly, because of the wide field

of view (50.6”), another radio source NGC 2024 FIR 6 is included in this observation. At last, the continuum image was produced using natural weighting, giving a synthetic beam of 1.30"×1.03". The rms of the clean continuum image is 4.6 mJy beam^{-1}.

Table 1: The observation data set details in this study.

Observation date	2022/11/09
Observation time	10:27-11:30 UTC
On source integration time	45 min
Target source	NGC 2024 FIR 5
Receiver setting	RxA 230 GHz
	RxB 240 GHz
Frequency range	
RxA lower side band	207.386 - 219.687 GHz
RxA upper side band	227.388 - 239.688 GHz
RxB lower side band	223.387 - 235.688 GHz
RxB upper side band	243.389 - 255.689 GHz
Target molecule	CO 2-1
Rest frequency	230.538 GHz
Number of antennas	8
synthesized beam size (max, min, pa)	1.30”, 1.03”, -84.65°

3. RESULTS

3.1. *Continuum emission*

Figure 1 shows the SMA continuum image of NGC2024 FIR 5 and FIR 6 at 1.3 mm with a resolution of 1.30"×1.03". The close-up image of FIR5 is presented in its upper-right panel. FIR 5 appears to be a single source in our observation. The peak flux density is 266 mJy/beam, while the total flux density is 0.51 Jy. Previous studies at 850 μm with a resolution of 2.45"×1.48" resolves a secondary peak located east to the main peak with a separation of ∼3" (Alves et al. 2011, see Figure 2). Nearby fainter sources FIR 5NE and FIR 5SW lie in north-east and south-west of the main structure are not detected as well compared with the 850 μm map. Furthermore, the elongation of FIR 5 is also different between the 1.3 mm data and the 850 μm data such that it is in northeast–southwest orientation viewed at 1.3 mm but appears in southeast–northwest orientation at 850 μm. Another structure missing in the 1.3 mm map is the Shell-like Southern Compact Peak (SCP) located in northern side of FIR5 seen at 6.9 mm continuum (Choi et al. 2012b, see Figure 3), which can be the result of lacking short spacing data in our observation, or that the 1.3 mm continuum mainly traces thermal dust emission as the SCP is reported to be an ionization front.

The lower-right panel of Figure 1 shows the close-up view of FIR 6 at 1.3 mm. The main object FIR 6C is caught along with the northern fainter object FIR 6N. The peak flux densities are 255 mJy/beam for FIR 6C and 48 mJy/beam for FIR 6N, while the total flux densities are 0.34 Jy for FIR 6C and 41 mJy for FIR 6N. Both sources appear to be compact sources similar as in previous studies at other wavelengths (e.g., Alves et al. 2011; Choi et al. 2012b).

3.2. *SED*

We perform SED analysis for NGC2024 FIR 5 and FIR 6C using total flux densities in different bands from our observation and literature with similar resolutions (Alves et al. 2011; Choi et al. 2012b; Wiesemeyer et al. 1997). FIR 6N is too faint to be detected in previous 3 mm and 6.9 mm observations. The total flux densities used are listed in Table 2. We plot the SEDs and linear fits in log-log scale in Figure 4. Best fits spectral indexes ($F_\nu \propto \nu^\alpha$) are α =2.60±0.48 for FIR 5 and 1.74±0.83 for FIR 6C. For FIR 5 the spectral index falls in the typical range for dust emission α, which indicate within the frequency range considered most of its flux comes from dust. SED of FIR 6C has a shallower slope mainly due to the decrease of the 850μm total flux density. Alves et al. (2011) argue that the smaller spectral index suggests the continuum consists primarily of free–free emission from the ultracompact HII region.

Alternatively, recent studies show the low spectral index can be due to the self-obscuration of optically thick dust in the envelope of embedded class 0/I YSOs or self-scattering of large (a_{max} ∼0.1 mm) dust grains (e.g., Li et al. 2017; Galván-Madrid et al. 2018; Liu 2019), although detailed modelling of the SEDs will be required to confirm these possibilities.

Table 2: Total flux densities of NGC FIR 5 and FIR 6C

Object	$S^{(a)}_{6.9m}$ (mJy)	$S^{(b)}_{3mm}$ (mJy)	$S_{1.3mm}$ (mJy)	$S^{(c)}_{850\mu m}$ (mJy)
FIR 5	9.1	249	513	3670
FIR 6C	3.8	112	340	116

NOTE— (a) Choi et al. (2012b), (b) Wiesemeyer et al. (1997), (c) Alves et al. (2011).

REFERENCES

Alves, F. O., Girart, J. M., Lai, S.-P., Rao, R., & Zhang, Q. 2011, ApJ, 726, 63, doi: 10.1088/0004-637X/726/2/63

Choi, M., Kang, M., Byun, D.-Y., & Lee, J.-E. 2012a, ApJ, 759, 136, doi: 10.1088/0004-637X/759/2/136

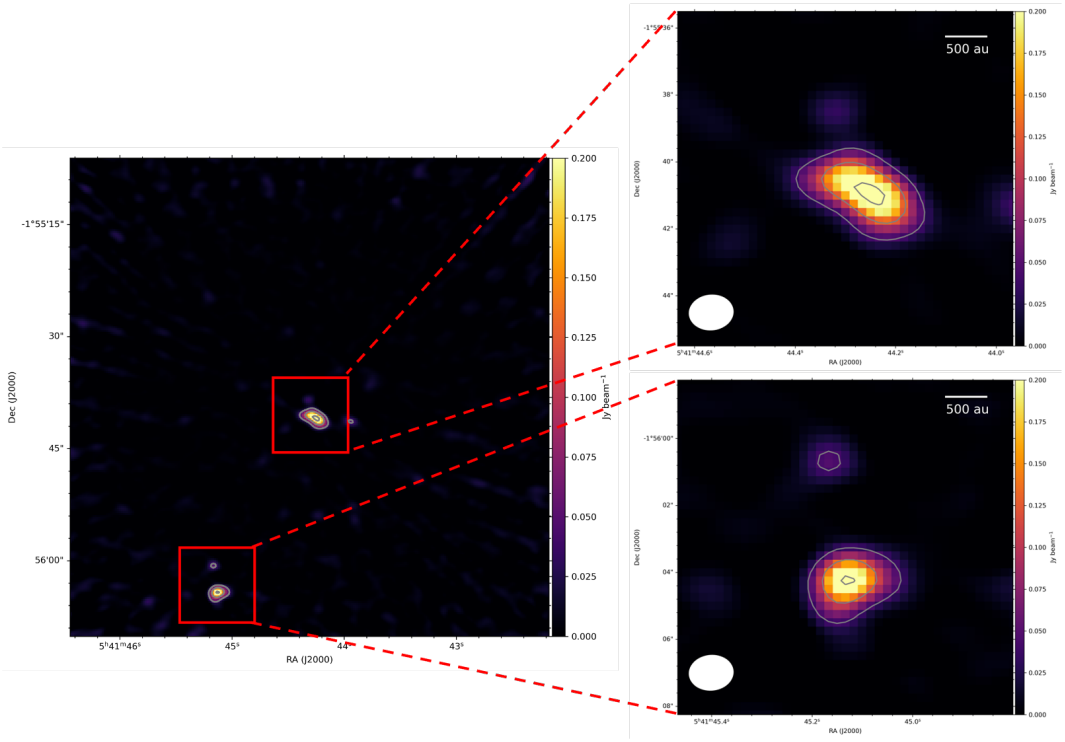

Figure 1: SMA Dust continuum image of NGC 2024 FIR 5 and FIR 6 at 1.3 mm and the close-up views. The synthesized beam is shown in the lower right corner. Contour levels are 4.4 mJy beam^{-1} (1σ) $\times$ [10, 30, 60].

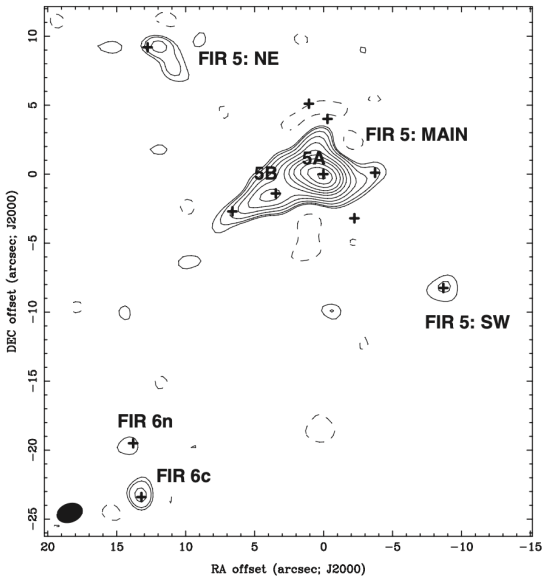

Figure 2: SMA Dust continuum image of NGC 2024 FIR 5 and FIR 6 at 850 μm The synthesized beam is shown in the lower left corner. Contour levels are 18 mJy beam^{-1} (1σ) $\times$ [-3, 3, 4, 6, 9, 13, 19, 25, 32, 42, 52, 62]. Image is extracted from Alves et al. (2011).

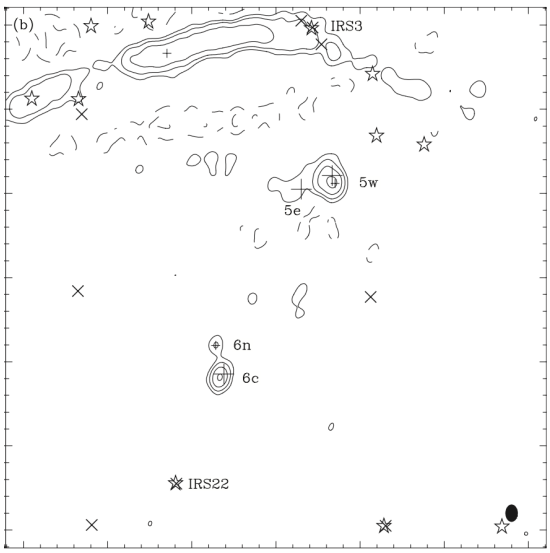

Figure 3: VLA Dust continuum image of NGC 2024 FIR 5 and FIR 6 at 6.9 mm. The synthesized beam is shown in the lower right corner. Solid contour levels are 0.3 mJy beam^{-1} $\times$ [1, 2, 4, 8, 16]. The rms noise is 0.12 mJy beam^{-1}. Image is extracted from Choi et al. (2012b).

148 Choi, M., Lee, J.-E., & Kang, M. 2012b, ApJ, 747, 112,
149 doi: 10.1088/0004-637X/747/2/112

150 Galván-Madrid, R., Liu, H. B., Izquierdo, A. F., et al. 2018, ApJ,
151 868, 39, doi: 10.3847/1538-4357/aae779

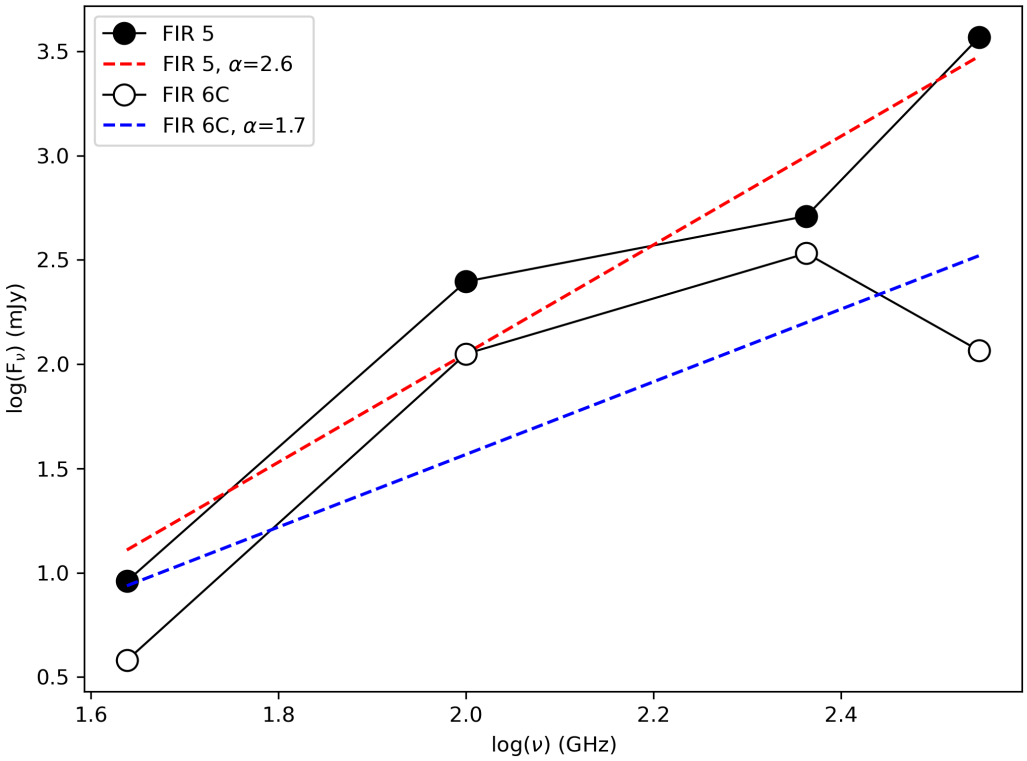

Figure 4: SEDs of FIR 5 (solid circles) and FIR 6C (open circles). Best fits of linear model in log-log scale are shown in red line for FIR 5 and blue line for FIR 6C. Uncertainties are smaller than marker sizes.

Li, J. I.-H., Liu, H. B., Hasegawa, Y., & Hirano, N. 2017, ApJ, 840, 72, doi: 10.3847/1538-4357/aa6f04

Liu, H. B. 2019, ApJL, 877, L22, doi: 10.3847/2041-8213/ab1f8e

Qi, C. 2003, in SFChem 2002: Chemistry as a Diagnostic of Star Formation, ed. C. L. Curry & M. Fich, 393

Richer, J. S. 1990, MNRAS, 245, 24P

Sault, R. J., Teuben, P. J., & Wright, M. C. H. 1995, in Astronomical Society of the Pacific Conference Series, Vol. 77, Astronomical Data Analysis Software and Systems IV, ed. R. A. Shaw, H. E. Payne, & J. J. E. Hayes, 433. https://arxiv.org/abs/astro-ph/0612759

Wiesemeyer, H., Guesten, R., Wink, J. E., & Yorke, H. W. 1997, A&A, 320, 287